# Energy & Environmental Science

Accepted Manuscript






ROYAL SOCIETY OF CHEMISTRY

www.rsc.org/ees

# TOC

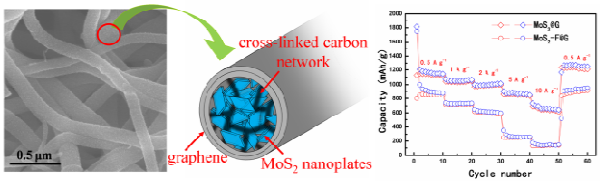


Text: one sentence, of maximum 20 words, highlighting the novelty of the work

A unique $MoS_2$@Graphene nanocable with novel contact model between $MoS_2$ nanosheets and graphene has been developed for high-performance lithium storage

Cite this: DOI: 10.1039/c0xx00000x

www.rsc.org/ees

COMMUNICATION

# Rational Design of $MoS_2$@Graphene Nanocables: towards High Performance Electrode Materials for Lithium Ion Batteries

**Debin Kong,[a,b,c‡] Haiyong He,[b‡] Qi Song,[b] Bin Wang,[b] Wei Lv,[c] Quan-Hong Yang[a,c]* and Linjie Zhi[a,b,c]***

***Received (in XXX, XXX) XthXXXXXXXXX 20XX, Accepted Xth XXXXXXXXX 20XX***

**DOI: 10.1039/b000000x**

**Here, we have successfully developed a novel contact mode between $MoS_2$ and graphene, where graphene rolls up into a hollow nanotube and thin $MoS_2$ nanosheets are uniformly standing on the inner surface of graphitic nanotubes, thus forming mechanically robust, free-standing, interwoven $MoS_2$@Graphene nanocable webs ($MoS_2$@G). Such a hybrid structure can maximize the $MoS_2$ loading in electrode in which over 90% of $MoS_2$ nanosheets with stacked layer number of less than 5 can be installed. Remarkably, when calculated on the basis of the whole electrode, this binder free electrode not only shows high specific capacity (ca. 1150 mA h $g^{-1}$) and excellent cycling performance (almost 100% capacity retention even after 160 cycles at a current density of 0.5 A $g^{-1}$) but exhibits a surprisingly high-rate capability of 700 mA h $g^{-1}$ at the rate of 10 A $g^{-1}$ despite of such a high $MoS_2$ loading content, which is one of the best results of $MoS_2$-based electrode materials ever reported thus far.**

Lithium ion batteries have proven successful in various portable electronics and are believed to be promising candidates for electric vehicles and grid energy storage as well, due to their high energy density, high voltage and environmental friendliness.[1-12] However, to achieve lithium ion batteries with excellent electrochemical performances such as high reversible capacity, stable cycle performance, and high rate capability, particularly for electric-vehicle applications, is known to be still hindered by the lack of suitable electrode materials. Thus, various electrochemically active materials have been recently investigated for lithium ion storage.[1, 3] Among these materials, Molybdenum sulfide ($MoS_2$) has received great attention as an anode material because it leads to a 4-electron transfer reaction during the charge/discharge process and achieves a capacity (around 669 mA h $g^{-1}$) two times that of the commercial graphite anode (372 mA h $g^{-1}$).[1, 13-16] However, the electric conductivity of $MoS_2$ is too low for its effective implementation as electrode, resulting in a poor rate performance of $MoS_2$ anode in most cases. Many efforts have been devoted to increase the conductivity of the whole electrode materials.[17-19] Among them, incorporation of carbonaceous materials with $MoS_2$ is the most effective way, by such as depositing $MoS_2$ sheets on carbonized organic conducting polymers[20] or carbon nanotubes,[21] and coating carbon onto $MoS_2$ using chemical vapor deposition (CVD)[22]. Due to the high electric conductivity, good flexibility and high chemical stability, graphene is believed as one of the most promising carbon matrices.[16, 23, 24] Graphene can also act as a "glue" to prevent the separation of the bulk active phase from the current collector even upon localized fracture. Chang[25] *et al.* reported a facile *in situ* solution-phase reduced method for growing $MoS_2$ layers on a graphene nanosheet in face-to-face mode to form graphene/$MoS_2$ hybrid, which exhibits high specific capacity of 1,100 mA h $g^{-1}$ at a current density of 0.1 A $g^{-1}$, as well as good cycling stability and high rate capability. Yang[23] *et al* further optimized a similar structure by designing three dimensional porous architectures constructed by graphene sheets coated with $MoS_2$ nanoplates, showing enhanced electrochemical performance. Interestingly, incorporation of $MoS_2$ with graphene may result in a capacity enhancement beyond the theoretical capacity (669 mA h $g^{-1}$), which can be contributed to the synergetic effect between the conducting graphene and $MoS_2$ and the storage of more Li both through adsorption (including at aromatic defects) and at the carbon-sulfide interfaces as well.[26-29] Unfortunately, such designing principle of face-to-face stacking between 2D nanoscale materials has generally been plagued by the relatively low content of $MoS_2$. It was reported that resistivity of $MoS_2$ through the basal planes is 2200 times larger as compared to the one parallel to the planes.[30] And thus the increase of $MoS_2$ loading would dramatically decrease the conductivity of electrode, when the $MoS_2$ combine with carbonaceous material via face-to-face contact. Nevertheless, the low mass loading of $MoS_2$ in the electrode results in the decrease of the gravimetric capacity and hence gravimetric energy density, fatally limiting the implementation of $MoS_2$ in a viable lithium ion battery. Thus, a new combination strategy between graphene and $MoS_2$ is of key importance for a high performance lithium ion battery.

Moreover, in traditional battery, an extra volume or weight percentage of up to about 30% is invalid due to the use of other

auxiliary components (e.g., binder, conductive carbon, foils) for only the purpose of better electric conductitity and better physical contacts, significantly reducing the volumetric capacity and gravimetric capacity of the overall electrode.[31, 32] Besides, the use of binder also introduces additional problems related to side reactions during the working cycles. Thus, recently, there has been an increasing interest in the development of binder-free and conductive additive-free film electrodes that can be directly used for lithium-ion batteries.[33-35] Electrospinning turns out to be a simple and versatile method for the large scale production of various flexible thin films composed of ultrathin nanofibers of various polymers composites, and even ceramics with such as hollow structures, porosities, and other morphologies.[36-38] Moreover, the resulting hollow fiber-based architectures possess high surface area, rich porous structures, and one-dimensional electron transport pathways. These features not only accommodate the volume change of metal oxides and sulfides but also facilitate the easy access to the electrolyte, and provide a continuous conductive network for the whole battery system.

In this work, we develop a novel contact mode between $MoS_2$ and graphene, as schematically shown in **Figure 1**a, where graphene rolls up into a hollow nanotube and thin $MoS_2$ nanosheets are uniformly standing on the inner surface of graphitic nanotubes, thus forming mechanically robust, free-standing, interwoven $MoS_2$@G nanocable webs. Surprisingly, such a hybrid structure can maximize the capability of active material $MoS_2$ loading for every individual nanocable in which over 90 % of $MoS_2$ nanosheets with stacked layer number of less than 5 can be installed. Due to the high $MoS_2$ loading as well as the excellent electric conductivity, the free-standing $MoS_2$@G webs can be used directly as binder free electrode in lithium ion batteries. Remarkably, this novel electrode not only shows high specific capacity (ca. 1150 mA h $g^{-1}$) and excellent cycling performance (almost 100% capacity retention even after 160 cycles at a current density of 0.5 A $g^{-1}$) but exhibits a surprisingly high-rate capability of 700 mA h $g^{-1}$ even at the rate of 10 A $g^{-1}$ despite of such a high $MoS_2$ loading content.

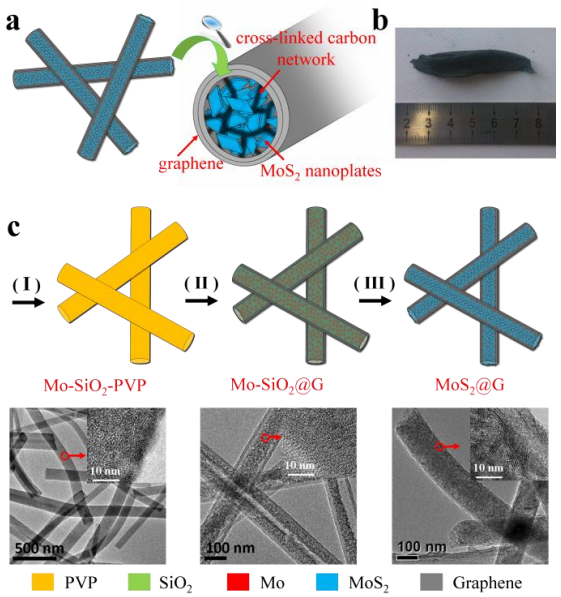


**Figure 1** Electrode design and fabrication. (a) The schematic diagram of $MoS_2$@G, where graphene rolls up into a hollow nanotube and thin $MoS_2$ nanosheets are uniformly standing on the inner surface of graphitic nanotubes. (b) obtained free-standing $MoS_2$@G membrane. (c) Schematic of the fabrication process of $MoS_2$@G, consisting of (I) electrospinning of the Polyvinyl pyrrolidone (PVP) solution with the addition of Molybdenum source and Tetraethylorthosilicate (TEOS), (II) depositing graphene through *in situ* decomposition of methane, and (III) annealing treatment in $H_2/H_2S$ and then removal of $SiO_2$.

The fabrication of such a proof-of-concept electrode prototype was realized through (I) synthesizing a flexible thin nanofibers web by electrospinning of Polyvinyl pyrrolidone solution containing Molybdenum source and Tetraethylorthosilicate, (II) depositing few layers of graphene on the surface of obtained nanofibers through *in situ* decomposition of methane, and (III) delaminating the resultant $MoS_2$@G hybrid membrane by annealing treatment in $H_2/H_2S$ and then removal of $SiO_2$ (**Figure 1**c). Notably, as shown in **Figure 1**a, despite the low carbon residue of PVP, an Ar atmosphere during the procedure (II) will still guarantee the formation of a cross-linked carbonaceous network among $MoS_2$ nanosheets in each nanocable, which is critically important for maintaining high specific capacity even at very high current densities. Besides, one batch of the prepared sample can easily reach 6 cm at length, which indicates the feasibility for scale up production (**Figure 1**b).

The morphology and microstructure of the as-prepared $MoS_2$@G nanocable webs through the above procedure have been investigated by means of scanning electron microscopy (SEM) and transmission electron microscopy (TEM). As shown in **Figure 2**a, the thus-produced hybrid web comprises an interconnected nanocables network and each nanocable is around 150 nm in diameter and several micrometers in length. The TEM images further demonstrate the nanostructure of each nanocable, wherein the cable wall consists of several layers graphene (average thickness: 5 nm) and the $MoS_2$ nanosheets are evenly embeded in a single nanocable (**Figure 2**b, c). The characteristic lattice fringe corresponding to 0.61 nm and 0.34 nm in the high resolution TEM images of $MoS_2$@G should be attributed to the (002) lattice of $MoS_2$ and the (002) lattice of multilayer graphene, respectively. The introduced graphene coating is suggested to be vital for maintaining the mechanical robustness and electricconnectivity of the web. As shown in Figure S1, graphene layers are grown on the surface of silica nanofiber through CVD process to form nanotubes. Notably, similar to the results reported previously by other research groups, graphene structures grown on silica substrate are not perfect graphene layers but multi-crystalline, defect-containing graphene structures.[39, 40] Actually，these characters of structure imperfections and defects are critically important for providing multiple pathways for efficient lithium ion transportation.[41]

It is observed that the domination of the number of stacked $MoS_2$ nanosheets are from 3 to 5 sheets in all the checked nanocables. Excitingly, such a stacking behavior of $MoS_2$ nanosheets makes the content of $MoS_2$ in the cable reaches up to over 90 wt%, as confirmed by TGA in **Figure S**3. Obviously, such a high $MoS_2$ loading is determined by the unique contact

mode of side to face between graphene and $MoS_2$ nanosheets. It's also worth noting that single or double sheets $MoS_2$ distribution can be realized as well but simply adjusting the content of $MoS_2$ to less than ca. 73 wt%, which is unfortunately relatively low for the application lithium ion batteries (**Figure S4**). As a comparison, a reference sample, $MoS_2$-F@G, is prepared by annealing treatment of $MoO_3$-$SiO_2$@G at $H_2S/H_2$ after the removal of $SiO_2$. Compared to $MoS_2$@G, $MoS_2$-F@G hold a similar Mo content as well as similar nanocables network but a quite different character in which large number of $MoS_2$ nanosheets are stacked heavily in each nanocable, as shown in **Figure 2**d, e. Besides, the size of the $MoS_2$ nanosheets of $MoS_2$@G is much smaller (ca. 10 nm in diameter) than that of $MoS_2$-F@G (tens or one hundred nm in diameter). The small diameter of $MoS_2$ nanosheets will obviously increase the number of the exposed electrochemically active sites, which will significantly enhance the ion diffusion efficiency during the reversible electrochemical reactions, as being demonstrated elsewhere.[42-44]

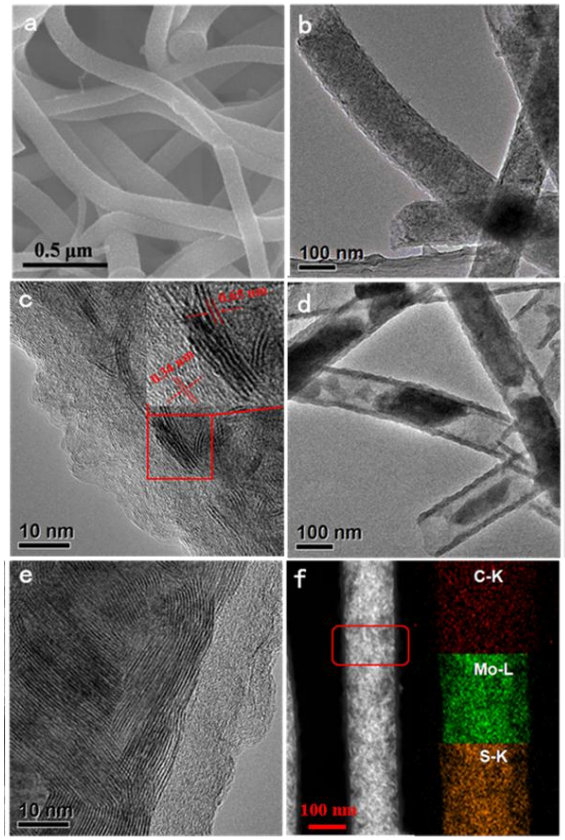


**Figure 2** (a) SEM images of a $MoS_2$@G; (b) TEM image of $MoS_2$@G; (c) High-magnification TEM images of $MoS_2$@G; (d) TEM image of $MoS_2$-F@G; (e) High-magnification TEM images of $MoS_2$-F@G; (f) Carbon, Molybdenum and sulfur elemental mapping of a selected area of an individual $MoS_2$@G. Scale bar, 100 nm.

Experimental investigations also indicate that $SiO_2$ has played a key role on the formation of $MoS_2$@G hybrid architectures. The presence of $SiO_2$ not only maintains the shape of the tube after the removal of PVP but also prevents the aggregation of formed $MoS_2$ nanosheets in the subsequent oxidation-sulfide process. Without the confinement effect of $SiO_2$, small $MoS_2$ nanosheets will grow and expand to tens or one hundred nanometers in diameter during the annealing process under $H_2S$ atmosphere, forming structures similar to that of $MoS_2$-F@G. Furthermore, owing to that there is no space between $SiO_2$ and graphene, the crystalline $MoS_2$ tend to grow along the space produced by decomposition and carbonization of PVP rather than along the graphene surface, so that most of the $MoS_2$ nanosheets are standing side to face on the inner surface of graphitic nanotubes. **(Figure S**5b). Besides, the mapping results of Mo, S and C elements further proves that ultrathin $MoS_2$ nanosheets distribute evenly in the entire nanocable for $MoS_2$@G (**Figure 2**f).

The detailed structure of $MoS_2$@G is further demonstrated by X-ray diffraction (XRD) and Raman analysis. The phase of hexagonal $MoS_2$ (Joint Committee on Diffraction Standards (JCPDS) No.: 37-1492) is clearly observed from the XRD patterns of the as-obtained nanocables, as shown in **Figure 3**a. The obvious broadening of its typical diffraction peaks is owed to the ultrathin dimension of $MoS_2$ nanosheets. It is rather remarkable that $MoS_2$-F@G possesses an obvious stronger response signal at $2\theta$ = 16 ° compared with that of $MoS_2$@G, which corresponds to the basal spacing of the heavily stacked $MoS_2$ nanosheets. For the Raman spectra, both samples show similar patterns as exhibited in **Figure S**6. In addition to the typical peaks of graphene (D peak at around 1350 $cm^{-1}$ and G peak at around 1600 $cm^{-1}$), the peaks at 376 and 402 $cm^{-1}$ belonging to the $MoS_2$ nanosheets are consistent with the Raman spectra of bulk $MoS_2$.[45]

The macro- and mesoporous feature of $MoS_2$@G hybrids has been demonstrated by nitrogen adsorption−desorption measurements. The adsorption data indicate the specific surface area of $MoS_2$@G is only 20 $m^2$ $g^{-1}$, reflecting the almost full filling of $MoS_2$ in the cables. Moreover, as shown in **Figure 3**b, $MoS_2$-F@G is obviously highly macroporous, due to the remaining space in the nanotube resulting from the heavy stacking of the $MoS_2$ nanosheets, which is in consistent with the TEM characterizations.

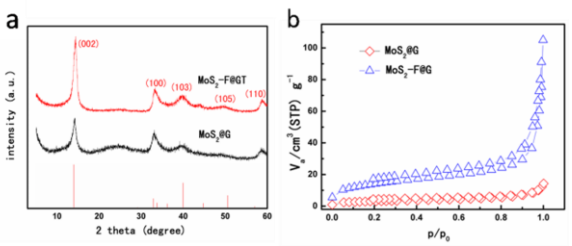


**Figure 3** Filling status and component analysis of $MoS_2$@G. (a) XRD patterns of $MoS_2$@G and $MoS_2$-F@G. (b) nitrogen adsorption−desorption measurements of $MoS_2$@G and $MoS_2$-F@G.

To evaluate the electrochemical properties of the $MoS_2$@G nanocable webs, two-electrode coin-type cells (2032) with metallic lithium counter electrodes have been fabricated using $MoS_2$@G and $MoS_2$-F@G as anode with no other additives. One molar $LiPF_6$ in 1:1 (v/v) ethylene carbonate/diethyl carbonate (EC/DEC) is used as the electrolyte. **Figure 4**a shows the representative cyclic voltammograms (CVs) of $MoS_2$@G

nanocables. It can be seen the CV behavior is generally consistent with that of $MoS_2$ reported previously[454443]. In the first cathodic sweep, peaks at approximately 0.8 V are observed and attributed to the formation of $Li_xMoS_2$ and the resulting 2H to 1T phase transition (reaction (1)). The large cathodic peak at approximately 0.4 V is attributed to the conversion reaction of $MoS_2$ to $Li_2S$ and molybdenum (reaction (2)). The irreversibility of this reaction is proven by the disappearance of these peaks in subsequent reduction cycles. Instead, a dominant cathodic peak at approximately 2.0 V is observed, while the peaks at 1.0 and 0.4 V previously discussed are greatly diminished in subsequent cycles. The dominant cathodic peak forming at ~2.0 V is well known in lithium–sulfur battery systems and is attributed to the formation of $Li_2S$. The dominant anodic peak at ~2.4 V is due to the conversion of $Li_2S$ to $S_8^{2-}$.[46, 47]

$$MoS_2 + xLi^+ + xe^- \longrightarrow Li_xMoS_2 \quad (1)$$

$$Li_xMoS_2 + (4 - x)\,Li^+ + (4 - x)\,e^- \longrightarrow Mo + 2Li_2S \quad (2)$$

Surprisingly, when being used as the anode of LIBs, a very high reversible capacity of about 1150 mA h $g^{-1}$ is achieved in the initial cycles at 0.5 A $g^{-1}$, in the case of $MoS_2$@G with 90% $MoS_2$ content (**Figure 4**b). We note that specific capacity of $MoS_2$ higher than 669 mA h $g^{-1}$ is well-documented in the literatures.[15, 16] It is shown that $MoS_2$ can take up to 8 lithium ions with major capacity between 0.01 to 1.0 V vs. $Li/Li^+$,[48] which corresponds to a theoretical capacity up to 1334 mA h $g^{-1}$. It is believed that the lithium ions can be stored in different defective sites of $MoS_2$ depending on the morphology of the material.[48] In addition, Cao[49] et al reported that the $MoS_2$ layers grown on three-dimensional graphene networks had a reversible capacity above 1000 mA h $g^{-1}$, and Chang[16] et al reported that the $MoS_2$/graphene composites could reach a capacity of 1200 mA h $g^{-1}$. We believe that the high capacity observed in our study is associated with the sufficient defects distribution of $MoS_2$@G and the synergetic effect between $MoS_2$ and graphene.

The coulombic efficiency (the ratio between charge capacity and discharge capacity) is 64% in the initial cycle, which rapidly reaches more than 99% after the second cycle. Even after 160 cycles, both the discharge and charge capacities of this material are stable at about 1150 mA h $g^{-1}$, delivering nearly 100% capacity retention. The excellent cycling stability can be mainly ascribed to the improved electric conductivity and the high structural stability of graphene-based nanocables network. As shown in **Figure S**7, the unique nanocable architecture can be well maintained even after 100 cycles. However, $MoS_2$-F@G revealed a relatively poor cycling stability (only 600 mA h $g^{-1}$ after 160 cycles), as shown in **Figure 4**b. Considering that the only difference between the two samples is the size of $MoS_2$ nanosheets and their stacking behaviors, the capacity decay on $MoS_2$-F@G probably arises from the generation of large particles from the heavy stacking of $MoS_2$ nanosheets during cycling, which influences both the formation of conductive networks and the diffusion dynamics of the lithium ions, suggesting an important role of the particle size of $MoS_2$ on the cycling ability.

The rate performance of LIBs is another critically important concern for practical applications, such as the commercial production of electric cars. **Figure 4**c shows the rate capability of $MoS_2$@G and $MoS_2$-F@G. Excitingly, the hybrid nanocables of $MoS_2$@G deliver an outstanding rate performance, revealing a reversible capacity of 1150 mA h $g^{-1}$ at a current density of 0.5 A $g^{-1}$ in the first cycle, and a capacity of around 700 mA h $g^{-1}$ even the current density increases to 10 A $g^{-1}$ (the corresponding full charge or discharge times are only 252 s). When the current density decreases to 0.5 A $g^{-1}$ after cycling under high current densities, $MoS_2$@G can still regain a reversible capacity near 1150 mA h $g^{-1}$. In sharp contrast, due to the limited ion diffusion arising from the heavily stacking of $MoS_2$ nanosheets for $MoS_2$-F@G, its reversible capacity fades rapidly to merely 200 mA h $g^{-1}$ at the current density of 10 A $g^{-1}$, and regains only around 25% of the initial capacity when the current density is reset to 0.5 A $g^{-1}$. More importantly, $MoS_2$@G exhibits very good cycling performance even at high current densities. As shown in **Figure 4**d, even after 700 cycles at 5 A $g^{-1}$, no capacity decay is observed. $MoS_2$@G can still offer a pretty high specific capacity up to 900 mA h $g^{-1}$. To the best of our knowledge, such an outstanding performance has never been reported previously on $MoS_2$-based electrode materials, which means that the here developed novel $MoS_2$@G is among the most promising anode materials for lithium storage and for high power Li-ion batteries (**Table S**1). It should be noted that such an excellent electrochemical performance is achieved on the basis of the whole electrode, free of any auxiliary components (e.g.,binder, conductive carbon, foils), which will significantly increase the gravimetric capacity for the final device in comparison to conventional LIBs.

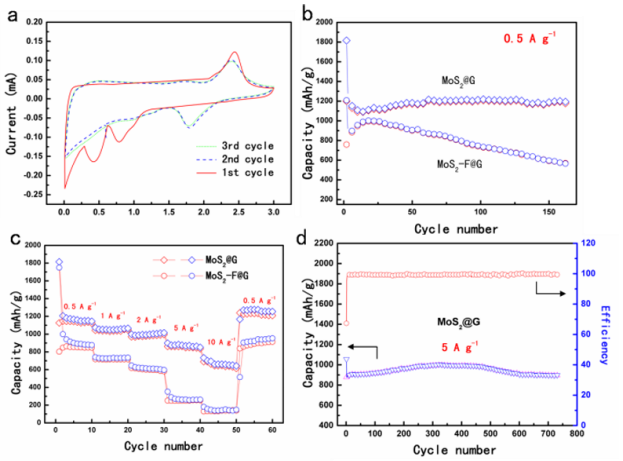


**Figure 4** (a) Representative CVs at a scan rate of 0.5 mV $s^{-1}$ for the first, second, and third cycles of $MoS_2$@G. (b) Electrochemical cycling performance of $MoS_2$@G and $MoS_2$-F@G electrodes under charge/discharge cycles from 3 to 0.1 V. (c) Reversible capacity of $MoS_2$@G and $MoS_2$-F@G at various current rates from 0.5 to 10 A $g^{-1}$. (d) Cycling performance and Coulombic efficiency of $MoS_2$@G at 5 A $g^{-1}$. All the capacities reported are on the basis of the whole electrode.

To gain an insight view for the reason of such excellent performance of $MoS_2$@G architecture, we conducted electrochemical impedance measurements (EIS) on $MoS_2$@G and $MoS_2$-F@G to reveal their electrochemical reaction kinetics. As shown in **Figure S**8, Nyquist plots show that the diameter of the semicircle for $MoS_2$@G in the high–medium frequency region is much smaller than that of $MoS_2$-F@G, indicating the greatly

decreased charge-transfer resistance at the electrode/electrolyte interface, which is resulted from the sufficient contact between the electrolyte and the uniformly distributed active $MoS_2$ nanosheets with small diameters. The high capacity, excellent cycle stability and rate capability of $MoS_2$@G nanocables could be attributed to the unique multiscale hybrid structures. First, in such structures, the flexible bulk film constructed by the interconnection of nanocables forms a strong skeleton framework and provides efficient electron transport pathways. Second, the nanocable walls of graphene with good mechanical properties can tolerate strain relaxation and accommodate the volume change of $MoS_2$ nanosheets, which effectively mitigates the stress and protects the active materials from pulverization during the discharge/charge process. Also worth noting is that even the content of $MoS_2$ is up to 90%, such a novel contact mode allows for the dominance of 3~5 layers of $MoS_2$ nanosheets, which avoid the aggregation of the active nanomaterials and retain small diameters and large surface area. Thus, nanoscale diameter and uniform dispersion of the $MoS_2$ nanosheets accelerate the Li-ion transport due to the shortened diffusion paths, resulting in excellent rate ability. Besides, the large contact area between nanocables and the electrolyte provides more active sites for $Li^+$ insertion/distraction. In general, this strategy sheds light on the utility of graphene as a building block to construct novel 2D/2D hybrid nanoarchitectures to improve significantly the electrochemical performance of a variety of metals, metal oxides, and sulfides.

In summary, we have successfully designed and prepared a novel $MoS_2$@G nanocable architecture to strike a balance between maximizing the $MoS_2$ content with small diameters and the effective conductive network of the entire system by introducing a unique side-to-face contact mode between graphene and $MoS_2$ nanosheets. When being used as an anode on the basis of the whole electrode, the $MoS_2$@G exhibits a specific capacity up to 1150 mA h $g^{-1}$ at 0.5 A $g^{-1}$ and an impressive rate capabilities with a capacity of 700 mA h $g^{-1}$ even at a current density of as high as 10 A $g^{-1}$, which means the corresponding full charge or discharge time of the cell is only 252 s. Remarkably, a pretty high capacity of 900 mA h $g^{-1}$ with a long cycle life (700 cycles with almost 100% capacity retention) at 5 A $g^{-1}$ are achieved, which belongs to one of the best results reported so far on $MoS_2$-based electrode materials. These results clearly demonstrate the advantage of the unique 2D@2D hybrid structures developed here, and further indicate a new protocol for developing 2D building blocks-based materials for high performance applications in energy storage devices, electrocatalysts, opto-electronics devices and other fields.

## Notes and references

[a] *School of Chemical Engineering and Technology, Tianjin University, Tianjin, 300072 (China)*
[b] *National Center for Nanoscience and Technology, No. 11 Beiyitiao, Zhongguancun, Beijing, 100190 (China)*
[c] *The Synergistic Innovation Center of Chemistry and Chemical Engineering of Tianjin, Tianjin, 300072 (China)*

*E-mail: zhilj@nanoctr.cn, qhyangcn@tju.edu.cn*

† Electronic Supplementary Information (ESI) available. See DOI: 10.1039/b000000x/
‡ Debin Kong and Haiyong He contributed equally to this work.
£ The authors would like to thank Bin Luo and Lin Shi for their help and discussions and the finance supports from the Ministry of Science and Technology of China (Nos. 2012CB933403 and 2014CB932403), the National Natural Science Foundation of China (Grant Nos. 20973044, 21173057 and 51372167), and the Chinese Academy of Sciences.

1 A. J. Heeger, *The Journal of Physical Chemistry B*, 2001, **105**, 8475-8491.
2 P. G. Bruce, B. Scrosati and J. M. Tarascon, *Angewandte Chemie International Edition*, 2008, **47**, 2930-2946.
3 A. S. Aricò, P. Bruce, B. Scrosati, J.-M. Tarascon and W. Van Schalkwijk, *Nature materials*, 2005, **4**, 366-377.
4 K. T. Nam, D.-W. Kim, P. J. Yoo, C.-Y. Chiang, N. Meethong, P. T. Hammond, Y.-M. Chiang and A. M. Belcher, *Science*, 2006, **312**, 885-888.
5 C. K. Chan, H. Peng, G. Liu, K. McIlwrath, X. F. Zhang, R. A. Huggins and Y. Cui, *Nature nanotechnology*, 2007, **3**, 31-35.
6 N. Recham, J.-N. Chotard, L. Dupont, C. Delacourt, W. Walker, M. Armand and J.-M. Tarascon, *Nature materials*, 2009, **9**, 68-74.
7 M. Armand, S. Grugeon, H. Vezin, S. Laruelle, P. Ribière, P. Poizot and J.-M. Tarascon, *Nature materials*, 2009, **8**, 120-125.
8 M. Morcrette, P. Rozier, L. Dupont, E. Mugnier, L. Sannier, J. Galy and J.-M. Tarascon, *Nature materials*, 2003, **2**, 755-761.
9 K. Kang, Y. S. Meng, J. Breger, C. P. Grey and G. Ceder, *Science*, 2006, **311**, 977-980.
10 B. Kang and G. Ceder, *Nature*, 2009, **458**, 190-193.
11 F. Zhang, T. Zhang, X. Yang, L. Zhang, K. Leng, Y. Huang and Y. Chen, *Energy & Environmental Science*, 2013, **6**, 1623-1632.
12 L. Zhang and X. W. Lou, *Chemistry – A European Journal*, 2014, **20**, 5219-5223.
13 R. Dominko, D. Arčon, A. Mrzel, A. Zorko, P. Cevc, P. Venturini, M. Gaberscek, M. Remskar and D. Mihailovic, *Advanced Materials*, 2002, **14**, 1531-1534.
14 H. Li, W. Li, L. Ma, W. Chen and J. Wang, *Journal of Alloys and Compounds*, 2009, **471**, 442-447.
15 J. Xiao, X. Wang, X.-Q. Yang, S. Xun, G. Liu, P. K. Koech, J. Liu and J. P. Lemmon, *Advanced Functional Materials*, 2011, **21**, 2840-2846.
16 K. Chang and W. Chen, *Chemical Communications*, 2011, **47**, 4252-4254.
17 S. Ding, D. Zhang, J. S. Chen and X. W. D. Lou, *Nanoscale*, 2012, **4**, 95-98.
18 A. Lynden, *Journal of Materials Chemistry*, 2012, **22**, 12988-12992.
19 X. Zhou, L.-J. Wan and Y.-G. Guo, *Nanoscale*, 2012, **4**, 5868-5871.
20 C. Zhang, Z. Wang, Z. Guo and X. W. Lou, *ACS Applied Materials & Interfaces*, 2012, **4**, 3765-3768.
21 S. Ding, J. S. Chen and X. W. Lou, *Chemistry – A European Journal*, 2011, **17**, 13142-13145.
22 C. Zhang, H. B. Wu, Z. Guo and X. W. Lou, *Electrochemistry Communications*, 2012, **20**, 7-10.
23 Y. Gong, S. Yang, Z. Liu, L. Ma, R. Vajtai and P. M. Ajayan, *Advanced Materials*, 2013, **25**, 3979-3984.
24 K. Chang and W. Chen, *ACS nano*, 2011, **5**, 4720-4728.
25 H. Hwang, H. Kim and J. Cho, *Nano letters*, 2011, **11**, 4826-4830.
26 C.-H. Lai, M.-Y. Lu and L.-J. Chen, *Journal of Materials Chemistry*, 2012, **22**, 19-30.
27 M.-R. Gao, Y.-F. Xu, J. Jiang and S.-H. Yu, *Chemical Society Reviews*, 2013, **42**, 2986-3017.
28 X. Huang, Z. Zeng and H. Zhang, *Chemical Society Reviews*, 2013, **42**, 1934-1946.
29 T. Stephenson, Z. Li, B. Olsen and D. Mitlin, *Energy & Environmental Science*, 2014, **7**, 209-231.
30 H. Wang, D. Kong, P. Johanes, J. J. Cha, G. Zheng, K. Yan, N. Liu and Y. Cui, *Nano letters*, 2013, **13**, 3426-3433.
31 J.-M. Tarascon and M. Armand, *Nature*, 2001, **414**, 359-367.

32 D. Liu and G. Cao, *Energy & Environmental Science*, 2010, **3**, 1218-1237.

33 D. Liu, B. B. Garcia, Q. Zhang, Q. Guo, Y. Zhang, S. Sepehri and G. Cao, *Advanced Functional Materials*, 2009, **19**, 1015-1023.

34 S. Luo, K. Wang, J. Wang, K. Jiang, Q. Li and S. Fan, *Advanced Materials*, 2012, **24**, 2294-2298.

35 C. Ban, Z. Wu, D. T. Gillaspie, L. Chen, Y. Yan, J. L. Blackburn and A. C. Dillon, *Advanced Materials*, 2010, **22**, E145-E149.

36 D. Li and Y. Xia, *Nano letters*, 2004, **4**, 933-938.

37 S. H. Nam, H.-S. Shim, Y.-S. Kim, M. A. Dar, J. G. Kim and W. B. Kim, *ACS Applied Materials & Interfaces*, 2010, **2**, 2046-2052.

38 W. Sigmund, J. Yuh, H. Park, V. Maneeratana, G. Pyrgiotakis, A. Daga, J. Taylor and J. C. Nino, *Journal of the American Ceramic Society*, 2006, **89**, 395-407.

39 J. Chen, Y. Wen, Y. Guo, B. Wu, L. Huang, Y. Xue, D. Geng, D. Wang, G. Yu and Y. Liu, *Journal of the American Chemical Society*, 2011, **133**, 17548-17551.

40 B. Wang, X. Li, X. Zhang, B. Luo, M. Jin, M. Liang, S. A. Dayeh, S. T. Picraux and L. Zhi, *ACS nano*, 2013, **7**, 1437-1445.

41 X. Li, Q. Song, L. Hao and L. Zhi, *Small*, 2014, **10**, 2122-2135.

42 N. Imanishi, K. Kanamura and Z. i. Takehara, *Journal of the Electrochemical Society*, 1992, **139**, 2082-2087.

43 J. Z. Wang, L. Lu, M. Lotya, J. N. Coleman, S. L. Chou, H. K. Liu, A. I. Minett and J. Chen, *Advanced Energy Materials*, 2013.

44 Y. Shi, Y. Wang, J. I. Wong, A. Y. S. Tan, C.-L. Hsu, L.-J. Li, Y.-C. Lu and H. Y. Yang, *Scientific reports*, 2013, **3**.

45 H. Liu, D. Su, R. Zhou, B. Sun, G. Wang and S. Z. Qiao, *Advanced Energy Materials*, 2012, **2**, 970-975.

46 X. Fang, X. Guo, Y. Mao, C. Hua, L. Shen, Y. Hu, Z. Wang, F. Wu and L. Chen, *Chemistry – An Asian Journal*, 2012, **7**, 1013-1017.

47 X. Fang, C. Hua, X. Guo, Y. Hu, Z. Wang, X. Gao, F. Wu, J. Wang and L. Chen, *Electrochimica Acta*, 2012, **81**, 155-160.

48 C. Feng, J. Ma, H. Li, R. Zeng, Z. Guo and H. Liu, *Materials Research Bulletin*, 2009, **44**, 1811-1815.

49 X. Cao, Y. Shi, W. Shi, X. Rui, Q. Yan, J. Kong and H. Zhang, *Small*, 2013, **9**, 3433-3438.